Item	Present?	Filename Whole original file name including extension. i.e.: Smith_SI.pdf. The extension must be .pdf	A brief, numerical description of file contents. i.e.: *Supplementary Figures 1-4, Supplementary Discussion, and Supplementary Tables 1-4.*
Supplementary Information	Yes	NATSUSTAIN-23010022B_SI.pdf	Supplementary Appendix 1, Supplementary Figs. 1–8, and Supplementary Tables 1–9.
Reporting Summary	Yes	NATSUSTAIN-23010022B_reporting-summary.pdf	
Peer Review Information	No	*OFFICE USE ONLY*	

Figure or Table # Please group Extended Data items by type, in sequential order. Total number of items (Figs. + Tables) must not exceed 10.	Figure/Table title One sentence only	Filename Whole original file name including extension. i.e.: Smith_ED_Fig1.jpg	Figure/Table Legend If you are citing a reference for the first time in these legends, please include all new references in the main text Methods References section, and carry on the numbering from the main References section of the paper. If your paper does not have a Methods section, include all new references at the end of the main Reference list.
Extended Data Fig. 1	**Nonlinear responses of multiple ecosystem variables to aridity.**	NATSUSTAIN-23010022B_ED_Fig1.jpg	**Nonlinear responses of multiple ecosystem variables to aridity.** Examples of aridity thresholds observed for NDVI (a), Vegetation fraction cover (b), Above-ground carbon density (c), Root-shoot ratio (d), Soil carbon content (e), Soil nitrogen content (f), Below-ground carbon density (g), Carbon sequestration (h), Biocrust cover (i), Inter-annual variation of precipitation (j), Plant species richness (k), and Vegetation sensitivity index (l). In (a.1) to (l.1), black

			dashed lines and black solid lines represent the smoothed trend fitted by a generalized additive model (GAM) and the linear fits at both sides of each threshold, respectively. The vertical grey dashed lines describe the aridity threshold identified. In (a.2) to (l.2), violin diagrams show bootstrapped slopes at the threshold of the two regressions existing at each side of the threshold values (yellow: regression before the threshold; red, after the threshold). Asterisks indicate significant differences when conducting a Mann-Whitney U test (two-sided) between before and after the threshold where: ***= P <0.001.
Extended Data Fig. 2	**Nonlinear responses of multiple ecosystem variables to grazing pressure.**	NATSUSTAIN-23010022B_ED_Fig2.jpg	**Nonlinear responses of multiple ecosystem variables to grazing pressure.** Examples of grazing pressure thresholds observed for NDVI (a), Vegetation sensitivity index (b), Above-ground carbon density (c), Plant species richness (d), Below-ground carbon density (e), and Sensitivity of vegetation to precipitation (f). In (a.1) to (f.1), black dashed lines and black solid lines represent the smoothed trend fitted by a generalized additive model (GAM) and the linear fits at both sides of each threshold, respectively. The vertical grey dashed lines describe the aridity threshold identified. In (a.2) to (f.2), violin diagrams show bootstrapped slopes at the threshold of the two regressions existing at each side of the

			threshold values (yellow: regression before the threshold; red, after the threshold). Asterisks indicate significant differences when conducting a Mann-Whitney U test (two-sided) of the data below and above the threshold where: ***= P value <0.001.
Extended Data Fig. 3	**Predicted areas with the difference between maximum allowable grazing pressure and current grazing pressure for the (a) contrasting effect or (b) synergistic effect of aridity and grazing pressure in China's drylands.**	NATSUSTAIN-23010022B_ED_Fig3.jpg	**Predicted areas with the difference between maximum allowable grazing pressure and current grazing pressure for the (a) contrasting effect or (b) synergistic effect of aridity and grazing pressure in China's drylands.** The blue and brown shading denotes where the maximum allowable grazing pressure is higher and lower than the current grazing level, respectively. The red lines denote the baseline drylands in 1950–2000 that are not suitable for grazing and thus where grazing is not recommended, as their maximum allowable grazing pressure is equal to zero and the current grazing pressure leads thresholds to be crossed for ecosystem attributes. The grey shading denotes drylands where the land covers are cropland, wetland or urban areas. The unshaded areas are not drylands today and therefore are outside of the range. The base map was obtained from the Global Aridity Index database[42] and China Data Lab[60].
Extended Data Fig. 4	**Future changes and climate change**	NATSUSTAIN-23010022B_ED_Fig4.jpg	**Future changes and climate change vulnerability in China's drylands.** a. Temporal variation in the mean aridity values across Chinese drylands. The thin

	vulnerability in China's drylands.		solid lines and shading are mean values and the 95% confidence intervals of the 20 CMIP5 climate models, respectively. Bold solid lines show the aridity trends by twenty-year running means. b. Projections of changes in the mean areas of four dryland subtypes (units: percentage of China's drylands) based on CMIP5 two representative concentration pathways (RCPs): RCP8.5 and RCP4.5 relative to the baseline period (1980–2014) for 2020–2060 and 2061–2100, respectively. Results are presented as mean values ± s.d. (n = 40). Error bars reflect the minimum and maximum number of area change with values equal to one standard derivation above and below the mean area change. The center of the error bar corresponds to the result calculated when the mean area change values are used. Changes include any transitions from the rest of three dryland subtypes to a subtype. Increased category includes any transitions to a subtype from the rest of three dryland subtypes (e.g., from dry sub-humid, semi-arid and arid to hyper-arid). Decreased category includes any transitions from a subtype to the rest of three dryland subtypes (e.g., from hyper-arid to dry sub-humid, semi-arid and arid).

Extended Data Fig. 5	**Predicted areas with the difference between maximum allowable grazing pressure and current grazing pressure in China's drylands under CMIP5 scenarios.**	NATSUSTAIN-23010022B_ED_Fig5.jpg	**Predicted areas with the difference between maximum allowable grazing pressure and current grazing pressure in China's drylands under CMIP5 scenarios.** a-b: CMIP5 scenarios RCP4.5 (i.e., assuming saturated increase in CO_2 emissions); a and b are for 2020–2060 and 2061–2100 relative to the baseline period (1980–2014), respectively. c-d: CMIP5 scenarios RCP8.5 (i.e., assuming sustained increase in CO_2 emissions); c and d are for 2020–2060 and 2061–2100 relative to the baseline period (1980–2014), respectively. The blue and brown shading denotes where the maximum allowable grazing pressure is higher and lower than the current grazing level, respectively. The red lines denote the baseline drylands in 1950–2000 that are not suitable for grazing and thus where grazing is not recommended, as their maximum allowable grazing pressure is equal to zero and the current grazing pressure leads thresholds to be crossed for ecosystem attributes. The grey shading denotes drylands where the land covers are cropland, wetland or urban areas. The unshaded areas are not drylands today and therefore are outside of the range. The base map was obtained from the Global Aridity Index database[42] and China Data Lab[60].

Extended Data Fig. 6	**Predicted areas with the difference between maximum allowable grazing pressure and current grazing pressure when aridity and grazing acted synergistically.**	NATSUSTAIN-23010022B_ED_Fig6.jpg	**Predicted areas with the difference between maximum allowable grazing pressure and current grazing pressure when aridity and grazing acted synergistically.** a-b: CMIP5 scenarios RCP4.5 (i.e., assuming saturated increase in CO_2 emissions); a and b are for 2020–2060 and 2061–2100 relative to the baseline period (1980–2014), respectively. c-d: CMIP5 scenarios RCP8.5 (i.e., assuming sustained increase in CO_2 emissions); c and d are for 2020–2060 and 2061–2100 relative to the baseline period (1980–2014), respectively. The grey shading denotes the baseline drylands in 1950–2000 that are unsuitable for grazing. The blue and brown shading denotes where the maximum allowable grazing pressure is higher and lower than the current grazing level, respectively. The red lines denote the baseline drylands in 1950–2000 that are not suitable for grazing and thus where grazing is not recommended, as their maximum allowable grazing pressure is equal to zero and the current grazing pressure leads thresholds to be crossed for ecosystem attributes. The grey shading denotes drylands where the land covers are cropland, wetland or urban areas. The unshaded areas are not drylands today and therefore are outside of the range. The base map was obtained from the Global Aridity Index database[42] and China Data Lab[60].

Extended Data Fig. 7	**Predicted areas with the difference between maximum allowable grazing pressure and current grazing pressure when aridity and grazing acted in opposition.**	NATSUSTAIN-23010022B_ED_Fig7.jpg	**Predicted areas with the difference between maximum allowable grazing pressure and current grazing pressure when aridity and grazing acted in opposition.** a-b: CMIP5 scenarios RCP4.5 (i.e., assuming saturated increase in CO_2 emissions); a and b are for 2020–2060 and 2061–2100 relative to the baseline period (1980–2014), respectively. c-d: CMIP5 scenarios RCP8.5 (i.e., assuming sustained increase in CO_2 emissions); c and d are for 2020–2060 and 2061–2100 relative to the baseline period (1980–2014), respectively. The blue and brown shading denotes where the maximum allowable grazing pressure is higher and lower than the current grazing level, respectively. The red lines denote the baseline drylands in 1950–2000 that are not suitable for grazing and thus where grazing is not recommended, as their maximum allowable grazing pressure is equal to zero and the current grazing pressure leads thresholds to be crossed for ecosystem attributes. The grey shading denotes drylands where the land covers are cropland, wetland or urban areas. The unshaded areas are not drylands today and therefore are outside of the range. The base map was obtained from the Global Aridity Index database[42] and China Data Lab[60].

Extended Data Table. 1	**The linear relationship between aridity (Ar) and maximum allowable grazing pressure (Gr) as determined by the two-dimensional threshold model which considers the combined effects of aridity and grazing pressure.**	NATSUSTAIN-23010022B_ED_Table1.jpg	**The linear relationship between aridity (Ar) and maximum allowable grazing pressure (Gr) as determined by the two-dimensional threshold model which considers the combined effects of aridity and grazing pressure.** The detailed descriptions of the line type are illustrated in Supplementary Fig.8.

Nature Sustainability thanks Jabed Tomal and the other, anonymous, reviewers for their contribution to the peer review of this work.

Editor summary:

Understanding the synergistic effects of aridity and grazing on dryland ecosystem attributes can be important for identifying ‘safe operating spaces’ for grazing under an increasingly arid climate. This study uses two-dimensional ecological threshold models to assess this in China’s drylands.

Climate-driven ecological thresholds in China’s drylands modulated by grazing

Changjia Li[1,2], Bojie Fu[1,2]*, Shuai Wang[1,2], Lindsay C. Stringer[3], Wenxin Zhou[1,2], Zhuobing Ren[1,2], Mengqi Hu[4], Yujia Zhang[5], Emilio Rodriguez-Caballero[6,7], Bettina Weber[7,8], Fernando T. Maestre[9,10]

1. State Key Laboratory of Earth Surface Processes and Resource Ecology, Faculty of Geographical Science, Beijing Normal University, Beijing, China
2. Institute of Land Surface System and Sustainable Development, Faculty of Geographical Science, Beijing Normal University, Beijing, China
3. Department of Environment and Geography, University of York, York, UK and York Environmental Sustainability Institute, University of York, York, UK
4. School of Mathematical Sciences, Beijing Normal University, Beijing, China
5. School of Statistics, Beijing Normal University, Beijing, China
6. Departamento de Agronomía, Universidad de Almería, Carretera Sacramento s/n, Almería, Spain
7. Multiphase Chemistry Department, Max Planck Institute for Chemistry, Mainz, Germany
8. Division of Plant Sciences, Institute for Biology, University of Graz, Graz, Austria
9. Instituto Multidisciplinar para el Estudio del Medio “Ramón Margalef,” Universidad de Alicante, Alicante, Spain
10. Departamento de Ecología, Universidad de Alicante, Alicante, Spain

*Corresponding author: bfu@rcees.ac.cn (B. Fu)

Habitat degradation of ecosystems can occur when certain ecological thresholds are passed below which ecosystem responses remain within ‘safe ecological limits’. Ecosystems such as drylands are sensitive to both aridification and grazing, but the combined effects of such factors on the emergence of ecological thresholds beyond which habitat degradation occurs has yet to be quantitatively evaluated. This limits our understanding on ‘safe operating spaces’ for grazing, the main land use in drylands worldwide. Here we assessed how 20 structural and functional ecosystem attributes respond to joint changes in aridity and grazing pressure across China´s drylands. Gradual increases in aridity resulted in abrupt decreases in productivity, soil fertility and plant richness. Rising grazing pressures lowered such aridity thresholds for most ecosystem variables, thus showing how ecological thresholds can be amplified by the joint effects of these two factors. We found that 44.4% of China’s drylands are unsuitable for grazing due to climate change induced aridification, a percentage that may increase up to 50.8% by 2100. 8.9% of current dryland grazing areas exceeded their maximum allowable grazing pressure. Our findings provide important insights into the relationship between aridity and optimal grazing pressure and identify ‘safe operating spaces’ for grazing across China’s drylands.

Main text

Drylands cover ~45% of Earth's land surface[1] and are home to about 40% of the world's population[2,3], providing a wide range of highly relevant ecosystem services (e.g., erosion control, climate regulation and supply of water, raw materials, and food), and harbor a unique biodiversity[4-6]. Dryland ecosystems are sensitive to ongoing global change drivers[7-11], which cause pressures that result in their degradation and desertification (Supplementary Fig. 1). Atmospheric aridity, a key climatic feature that is increasing worldwide due to global warming, affects key ecosystem attributes and functions in global drylands[11-14], causing systemic and abrupt changes in multiple ecosystem variables[11,14,15]. Such changes often occur when certain thresholds are passed[16,17], below which ecosystem responses remain within 'safe ecological limits'[18]. Once thresholds are passed, ecological responses are characterized by having a disproportionately increasing magnitude and variance[19]. Determining such potential thresholds is key for identifying early warning signals of possible catastrophic shifts, and for developing sustainable environmental management programs and climate change adaptation strategies.

Managed livestock grazing, which occurs in ~65% of global drylands[20], may affect plant community composition and ecosystem functioning in a similar way as aridity[20]. Drivers of ecosystem structure and functioning in drylands, such as climatic conditions and grazing pressure, rarely act independently, and interactions among them may act synergistically or in opposition[21-24]. However, very few studies have considered the joint effects and potential interactions between aridity and grazing on the response of ecosystem variables[20,22,25], and none has evaluated whether and how they jointly shape ecological thresholds in drylands. Understanding how ecosystem structure and functioning change in response to joint changes in aridity and grazing pressure is important for advancing ecological threshold theory, and for identification of the maximum allowable grazing pressure levels that drylands can support (i.e., the 'safe operating space' for grazing) before degrading under specific aridity levels. This information is particularly relevant to guide the management of grazing across drylands worldwide.

Here we used >20,000 data points from 20 ecosystem functional and structural variables to test the hypothesis that grazing pressure acts synergistically with aridity to modify the ecosystem thresholds driven by aridity across Chinese drylands. To test this hypothesis, we evaluated physical (e.g., albedo, soil texture, and precipitation variability), chemical (e.g., soil organic carbon and leaf nitrogen), and biological (e.g., plant cover, richness, and functional traits) ecosystem attributes, and adapted a two-dimensional threshold model to evaluate their responses to aridity under different levels of grazing pressure. We focus on China because it contains one of the largest dryland areas -6.6 million km^2- worldwide[1], which provide essential goods and services to approximately 580 million people[26]. Chinese drylands are at risk of expansion or have already expanded[27,28], and account for one third of the expansion of global drylands during 1980-2000[29]. Grazing occurs in 76% of China's drylands, supports local livelihoods, and is highly linked to the sustainable development of these areas[26]. By assessing how China's drylands respond to joint changes in aridity and grazing we aimed to: i) identify optimal grazing pressure (i.e., the grazing pressure drylands can support before degrading) under different aridity conditions, ii) highlight which areas are exceeding their maximum allowable grazing pressure, and iii) predict potentially vulnerable areas that will cross their maximum allowable grazing pressure identified due to climate change by 2100.

Results

Most functional and structural ecosystem attributes evaluated exhibited a non-linear relationship with aridity and grazing (Extended Data Fig. 1-2, Supplementary Table 3 and 5). Both factors had convergent and contrasting effects on dryland ecosystem structure and functioning. In most cases, both aridity and grazing caused reductions in vegetation properties including plant cover and species richness (Fig. 1a and b), and in soil carbon and nitrogen contents (Fig. 1c and d). When considering them together, aridity and grazing had a synergistic effect on most structural and functional ecosystem variables, and grazing modified the observed aridity thresholds (Supplementary Table 6 and 3). For example, the aridity threshold for plant cover was 0.74, but decreased to 0.68 when considering the combined effect of aridity and grazing, with a further decrease observed with increases in grazing pressure. These results indicate that ecological thresholds are amplified by the joint effects of increasing aridity and grazing pressure.

Despite this overall trend, aridity and grazing had contrasting effects on the above-ground carbon density and carbon sequestration capacity: increases in aridity led to a decrease in above-ground carbon density and carbon sequestration, but increases in grazing pressure were positively correlated with these variables (Fig. 1e and f). The observed aridity thresholds were higher when considering the combined effect of aridity and grazing than when considering aridity alone (Supplementary Table 6 and 3). These results suggest that in some cases, grazing could reduce the negative effect of increases in aridity by promoting plant productivity. For other variables, such as biocrust cover and inter-annual precipitation variability, grazing did not affect the aridity thresholds observed (Fig. 1g and h).

For most variables that showed a decreased trend with increasing aridity (i.e., plant cover and species richness), a negative relationship was observed between aridity and optimal grazing pressure (Fig. 2a). The maximum allowable grazing pressure decreased by 2.4% per 0.01 increase in aridity. 44.4% of Chinese drylands (279.8 x 10^4 km^2), mostly located in the northwestern arid and hyper-arid regions (Fig. 3a), had a maximum allowable grazing pressure equal to zero. These results indicate that ecosystem attributes (i.e., vegetation cover, soil nitrogen content and plant species richness) are crossing ecological thresholds under the current grazing pressure levels experienced by these areas. These regions were thus identified as places where grazing is not recommended. 8.9% of drylands (56.3 x 10^4 km^2, 96.5% of which occurring in semi-arid regions) presented their maximum allowable grazing pressure at a lower level than that at which they are currently grazed, indicating that those are the priority areas where grazing pressure should be reduced. Remaining areas (22.3% of total drylands in China), mainly distributed in the southwestern and northeastern semi-arid and dry sub-humid regions, had a higher maximum allowable grazing pressure than their current grazing levels and thus have room for increasing the stocking rate. In addition, the interaction between aridity and grazing pressure with the reductions of aridity thresholds as grazing pressure increases (Tline1_1, synergistic effect, Supplementary Fig. 8c) led to 46.6% of China´s dryland area not being recommended for grazing (Extended Data Fig. 3a).

Predicted increases in aridity under RCP4.5 and RCP8.5 scenarios (Extended Data Fig. 4) are expected to cause spatial and temporal changes in maximum allowable grazing pressure in China’s drylands (Fig. 3b). Compared to the historical period (1980–2014), ongoing aridification will lead to a 1.4% increase in the areas where grazing is not recommended, summing up to a total of 45.8% of China’s drylands for the time-span 2020-2060. Considering the 2061-2100 period, the increase sums up to a total of 50.8% of China´s drylands (Fig 3, Extended Data Fig. 5). In addition, areas with potential for an increasing stocking rate during 2061-2100 decreased from 22.3% to 19.7% and 18.3% under RCP4.5 and RCP8.5 scenarios, respectively (Fig 3c and d). The synergistic effect of future aridity and current grazing pressure increased the area where grazing is not recommended to 53.0% by 2100 (Extended Data Fig. 6). When aridity and grazing pressure acted in opposition for several ecosystem variables (i.e., above-ground carbon density and carbon sequestration) that showed thresholds occurring at higher aridity levels as grazing pressure increases (Tline1_2, contrasting effect, Supplementary Fig. 8c), the area in which the stocking rate could be increased declined from 24.9% to 20.3% by 2100 (Extended Data Fig. 7).

Soil texture also modified the observed ecosystem thresholds driven by aridity and grazing pressure (Supplementary Tables 7 and 8). As sand content increased from low to high, ecosystem variables such as vegetation and biocrust cover, above-and below-ground carbon density, soil carbon and nitrogen content showed a smaller aridity threshold, while the aridity threshold for NDVI and plant species richness increased by 0.30 and 0.38, respectively (Supplementary Table 7). High sand contents delayed the threshold of grazing pressure by 26 grazing livestock units per km^2 (Supplementary Table 8). These findings illustrate how increases in sand content interact with aridity and grazing pressure to either increase or decrease ecosystem responses to these factors.

Discussion

Aridity had a predominantly negative effect on ecosystem structure and functioning across China's drylands, whereas the effects of grazing ranged from weaker negative to positive or neutral, depending on the ecosystem attributes evaluated (Fig. 2). Overall, a gradual increase in aridity led to abrupt decrease in productivity, soil fertility, and plant richness at aridity values of 0.7, 0.8 and 0.95, respectively (Supplemental Appendix 1). However, increases in grazing pressure made aridity thresholds occur at lower aridity values for most ecosystem variables, suggesting that increases in grazing pressure make drylands more prone to suffer abrupt shifts in their structure and functioning.

A global meta-analysis[30] also reported that the negative effects of grazing pressure on plant species richness were larger in arid than in sub-humid regions. However, the present findings disagree with the pattern previously proposed showing that the effect of grazing pressure on plant species richness increased with decrease in aridity[31]. The main reason for this difference is that more species with diverse adaptive traits are found in more humid ecosystems, so grazing induces strong changes in species composition[31,32] with subtle change in species richness[30]. We also found that aridity and grazing imposed convergent selective pressures on vegetation attributes (characterized by decline in vegetation cover and plant species richness) (Fig. 2c), suggesting that aridity-resistant species are also grazing-resistant species[20]. Physiological mechanisms of plant adaptation to water stress in more arid environments typically include shorter plant height, smaller and harder leaves, and lower N content (lower palatability), which lead to resistance to drought and defenses against herbivory [32-34]. Aridity enhanced the negative effects of overgrazing on ecosystem structure and functioning. These synergistic negative effects of aridity and grazing will be enhanced in the future given forecasted increases in aridity (15.3% increase by 2100; Extended Data Fig. 6), further reducing the capability of China's drylands to provide essential ecosystem services.

The responses of above-ground carbon density and carbon sequestration capacity to aridity and grazing showed a different pattern, with positive effects of grazing and negative effects of aridity. A potential mechanism behind the positive correlation between grazing pressure and above-ground carbon density is that grazing may promote encroachment by woody plants and thus results in increased above-ground carbon density[35]. The contrasting effects of aridity and grazing pressure observed are partly explained by competitive exclusion or rare species under no grazing or low grazing pressure conditions, particularly in less arid environments where competition for light is exacerbated[31]. In this study, the focus was mainly on low to moderate intensity grazing, as the studied grazing pressure level was mostly <200 grazing livestock units per km^2, which is consistent with the realistic ranges of stocking rates for low (158±76, n=18) and moderate (325±162, n=20) grazing pressure levels (Supplementary Table 9). Low to moderate grazing pressure reduces palatable grasses and promotes the dominance of grazing-tolerant shrubs that have denser cover and higher carbon sequestration capability[20,36]. These results suggest that maintaining and enhancing biotic attributes (i.e., vegetation and biocrust cover, and plant species richness) with appropriate livestock management, including increasing stocking rate by 92±37 livestock units per km^2 in the 22.3% of drylands where the maximum allowable grazing pressure is higher than the current grazing pressure, could buffer the negative effects of the ongoing climate change and aridity on ecosystem functioning in these areas.

Overall, our results indicate that the effects of aridity and grazing pressure cannot be evaluated in isolation, and highlight the importance of considering grazing pressure when assessing dryland responses to changes in climatic conditions. They also suggest that current grazing pressure is likely to enhance the risk of environmental degradation caused by aridification in 50.8%-55.7% of China's drylands (Extended Data Fig. 3). Both abiotic and biotic mechanisms are associated with the occurrence of a grazing threshold. Grazing tends to reduce the cover of palatable grasses and induces a relative increase in the cover of unpalatable grasses and shrubs[20]. The recognition that real threshold changes exist across grazing gradients can help land managers to prevent the occurrence of land degradation due to overgrazing. Our analyses captured the relationship between aridity and optimal grazing pressure that falls within 'safe operating spaces' within Chinese rangelands (Fig. 2), providing a suitable framework for identifying such spaces at regional or global scales where data is available.

Our study has important implications for the sustainable management of rangeland ecosystems, which account for 34.2% China's total dryland area[26]. In most cases, optimal grazing pressure decreased with aridity, so grazing is not recommended in 44.4% of China's drylands under current grazing pressure levels, and will not be recommended in 50.8% of the country's drylands by 2100 (Fig. 3). Specifically, reducing grazing pressure by 24±38 livestock units per km^2 in 53.4% of drier environments, including 44.4% of areas with no grazing and 8.9% areas with lower maximum allowable grazing pressure, could be an effective measure to reduce the risk of land degradation and desertification in these areas. However, keeping a moderate and optimal grazing pressure by increasing 92±37 livestock units per km^2 in wetter environments (22.3% of drylands) is key to enable production of meat, milk and leather, thereby supporting local livelihoods, and to enhance species richness and both ecosystem multifunctionality[36] and services[24]. In addition, rangeland management activities should aim, whenever possible, to enhance plant species richness to alleviate the negative effects of ongoing increases in temperature being experienced in many Chinese drylands.

In our study, log transformation of the variables was used to reduce the conditional variance across the aridity and grazing gradients evaluated. Quantile regressions were used to focus on the central tendency of the variable following a bimodal distribution, rather than on the mean, to correct the maximum likelihood estimation of the linear model that relies on the ordinary least squares of the residuals. These methodological approaches are highly suitable for identifying thresholds in response variables[37,38], and have been widely used in ecological studies[11,39,40]. Nevertheless, future model improvements could incorporate and estimate the changes in the conditional locations of the analyzed response variables directly into the models via conditional variance, based on more robust estimations[39].

Our study provides insights that are crucial to guide adaptation and management actions to maximize the socio-ecological benefits of grazing while preventing current and future land degradation and desertification. In doing so, appropriate actions on grazing could help to secure the livelihoods of approximately 580 million people living within and in the vicinity of China's drylands[26]. Our findings also contribute to the prediction of possible ecosystem responses to future changes in climate and land use intensity in Chinese and similar drylands worldwide.

Methods

Data collection

We selected a set of 20 variables (Supplementary Figs. 2–4, Supplementary Table 1) that are key for determining ecosystem structure and functioning in drylands, as well as their capacity to deliver essential ecosystem services[11,41]. These variables included physical (e.g., albedo and inter-annual precipitation variability), biological (e.g., vegetation cover and productivity, plant species richness, and biocrust cover), and chemical (e.g., soil organic carbon and leaf nitrogen) ecosystem attributes. We defined drylands as regions where the aridity index (*AI*), which is the ratio of annual precipitation to potential evapotranspiration[3,26], is below 0.65, with four dryland subtypes including hyper-arid ($AI < 0.05$), arid ($0.05 \leq AI < 0.20$), semi-arid ($0.20 \leq AI < 0.50$) and dry sub-humid ($0.50 \leq AI < 0.65$)[26].

We obtained interpolated and remote sensing data by sampling one point every 12 arc-minutes of the area covered by drylands in China using publicly available maps (Supplementary Table 1). All points classified as urban, cultivated lands or water bodies by FAO were excluded, resulting in 12,450 points covering grasslands, shrublands, deserts, and forests. At each point, we extracted the following variables, which have an important role in affecting dryland climate, ecosystem structure and functioning: i) *Aridity (1-AI)*, which was retrieved from the Global Aridity Index database[42]; ii) *Albedo*: White Sky Albedo (*WSA*) for shortwave spectral domain (i.e., 0.3-5 μm) was retrieved from MODIS MCD43D61–MODIS/Terra+Aqua BRDF/Albedo White Sky Albedo Shortwave Daily L3 Global 30ArcSec CMG dataset[43]. *WSA* was evaluated daily from May to September between 2000–2015, then averaged on a yearly basis for the entire study period to avoid effects associated with seasonal and yearly differences; iii) *Inter-annual precipitation variability*: The coefficient of variation (*CV*) of precipitation is commonly used to estimate inter-annual precipitation variability. Annual precipitation was obtained from TerraClimate datasets[44] and *CV* of annual precipitation rainfall (standard deviation/mean) was calculated for the 1980-2015 period; iv) *Soil variables* include soil carbon content, soil nitrogen content, soil C/N ratio, and silt and clay content, and were obtained from the harmonized soil database WISE30sec[45]; v) *Plant productivity*: The Normalized Difference Vegetation Index (*NDVI*) was used to represent plant productivity, as it indicates the photosynthetically active radiation absorbed by plant canopies. *NDVI* data was acquired from the SPOT/VEGETATION NDVI satellite remote sensing product[46] on a monthly basis (generated using the maximum value of *NDVI* data with a ten-day temporal resolution) between

January 2000 and December 2015, and was averaged for the entire period; vi) *Vegetation cover*: Vegetation cover was obtained from the MODIS MOD44B remote sensing product[47] to estimate tree and non-tree vegetation cover; vii) *Occurrence of shrublands*: The occurrence of shrublands was used to evaluate their encroachment with changes in aridity. This variable was calculated by creating a binary data set with values 1 or 0, indicating that for a given point the land is covered by open or dense shrubland or other vegetation types, respectively. When changes in the dominant vegetation were observed over time (i.e., from shrubs to other vegetation types or from others to shrubs), we kept the most representative (i.e., the land type recorded during most years for the period between 1980 and 2015) for each site. The data on vegetation type were obtained using the time series Landsat TM/ETM remote sensing maps (https://landsat.gsfc.nasa.gov/), recorded in 1980, 1990, 1995, 2000, 2005, 2010 and 2015, and was retrieved from the Resource and Environmental Data Cloud Platform (https://www.resdc.cn/Default.aspx); viii) *Biocrusts*: biocrust occurrence was derived from the global distribution of biocrusts obtained by application of environmental niche modelling based on field observations reported in more than 500 publications and identification of 18 independent environmental parameters controlling the suitability of the land surface for the growth of biocrust[48]; ix) *Plant species richness* was obtained from a previous study by Ellis, et al. [49] who quantified vascular plant species richness through use of spatially explicit models and estimating native species loss with replacement with exotic species caused by species invasions and the introduction of agricultural domesticated and ornamental exotic plants [Native Species Richness – Anthropogenic Species Loss + Anthropogenic Species Increase (Species Invasions + Crop Species + Ornamental Species)]; x) *Sensitivity of Vegetation to Precipitation (SVP)*, which was defined as the slope of regression between *NDVI* and precipitation. The SVP index reflects changes in the structural and functional ecosystem state that leads to environmental deterioration[50]. The sequential dynamics of *SVP* can be calculated with Sequential Regression (SeRGs) applied in moving windows (see full details in the Supplementary Appendix 2 of Li, et al. [26]). In general, the moving windows involved a spatial dimension (1, 3, 5, 7, 9 pixels) and temporal dimension (1, 2, 3, 4, 5, 6, 7, 8, 9, 10, 11 years). For each of the spatial and temporal windows, the percentage of significant relationships ($p < 0.1$) between annual *NDVI* and precipitation was calculated, and the optimal combination of spatial and temporal windows was then selected with the criterion that as many significant relationships as possible were contained in the smallest possible space-time window[51]. A spatial dimension of 3 pixels and a temporal dimension of 9 years were selected as the optimal threshold resulting in more than 90% of significant relationships in all tested moving windows with the smallest window size; xi) *Vegetation sensitivity index (VSI): VSI* is a metric that compares the relative variance of enhanced vegetation index (*EVI*, a vegetation index similar to NDVI) with water availability, air temperature and cloud-cover. VSI is used to determine the sensitivity of vegetation to climatic fluctuations including precipitation and temperature changes, and is considered as an important index of vegetation resilience. *VSI* values were obtained from Seddon, et al. [10], and original data for each year between 2000 and 2013 were averaged for the entire period, with a spatial resolution of 5 km[10]; xii) *Ecosystem functions*: Data on water yield, soil conservation, carbon sequestration and habitat quality in China's drylands were obtained from Xu, et al. [52], who used the InVEST model and land use, climate and soil data as inputs to quantify multiple ecosystem services generated by a landscape; xiii) *Grazing pressure* was expressed as the sum of the number of livestock units (animals·km^{-2}) obtained from the Gridded Livestock of the World (GLW) database[53]. The GLW database provided a reasonable and accessible global map on the distribution and abundance of livestock, using regression-based methods to model global livestock densities at a spatial resolution of 3 arc - minutes (about 5×5 km at the equator)[54,55]. Here we aggregated the estimated density of sheep, goats and cattle which are the major type of livestock found across China's drylands; and xiv) *Root-shoot ratio* was derived from a global database involving 17,814 plot-level root mass measurements, composed of 6803 individual samples from 5170 forest, 1293 grassland and 340 shrubland sites[56]. For China's drylands, we have 3051 root-shoot ratio measurements, covering 1879 forest sites, 998 grassland sites and 174 shrubland sites.

Data analyses

Two-dimensional threshold model

To evaluate the joint effects of aridity and grazing pressure on ecosystem attributes, we adapted a two-dimensional threshold model based on the traditional one-dimensional threshold model (Supplemental Appendix 1 and Supplementary Fig. 6)[11]. Basically, there are two types of thresholds: continuous and discontinuous, which define a threshold line as the linear relationship between aridity and optimal grazing pressure in which a given ecosystem variable either abruptly changes its value (discontinuous threshold) or does not (continuous threshold). We fitted threshold models including hinge, upper hinge, segmented, step, and stegmented regressions to determine the thresholds (detailed in Equations (1-5) and Supplementary Fig. 7a-e, respectively). Hinge, upper hinge, and segmented regressions are continuous, whereas step and stegmented regressions are discontinuous[57]. Hinge regression is a linear discontinuous regression with changes in the intercept and slope (a 0 used for one fitted plane) at both sides of a threshold line. Upper hinge regression is a linear discontinuous regression with changes in both the intercept and slope (expressed as 0 for one fitted plane) at both sides of a threshold line. Segmented regression is a linear continuous regression with a change in the slope (not 0 for both fitted planes) at a threshold line. Step regression is a linear discontinuous regression that exhibits a change only in the intercept but has its slope as 0 at both sides of the threshold line. Stegmented regression is a linear discontinuous regression that exhibits changes in both the intercept and slope at the threshold line. The regression functions were expressed using the following equations:

Hinge:

$$\mathrm{Var} = \beta_0 + \beta_1 I[f(AI, GI, e_{AI}, e_{GI}) > 0] \cdot f(AI, GI, e_{AI}, e_{GI}) \quad (1)$$

Upper hinge:

$$\mathrm{Var} = \beta_0 + \beta_1 I[f(AI, GI, e_{AI}, e_{GI}) < 0] \cdot f(AI, GI, e_{AI}, e_{GI}) \quad (2)$$

Segmented:

$$\mathrm{Var} = \beta_0 + \beta_1 I[f(AI, GI, e_{AI}, e_{GI}) > 0] \cdot f(AI, GI, e_{AI}, e_{GI}) + \beta_2 AI + \beta_3 GI \quad (3)$$

Step:

$$\mathrm{Var} = \beta_0 + \beta_1 I[f(AI, GI, e_{AI}, e_{GI}) > 0] \quad (4)$$

Stegmented:

$$\mathrm{Var} = \beta_0 + \beta_1 I[f(AI, GI, e_{AI}, e_{GI}) > 0] \cdot f(AI, GI, e_{AI}, e_{GI}) + \beta_2 AI + \beta_3 GI + \beta_4 I[f(AI, GI, e_{AI}, e_{GI}) > 0] \quad (5)$$

where AI and GI represent aridity and grazing pressure, e_{AI} and e_{GI} are two threshold parameters related to the predictors of AI and GI, Var represents the various variables (e.g., inter-annual precipitation variability, vegetation cover, vegetation sensitivity index), and $f(\mathrm{AI}, \mathrm{GI}, e_{AI}, e_{GI})$ is the threshold function[58] which is presented in the following equations:

$$f(AI, GI, e_{AI}, e_{GI}) = \begin{cases} \frac{AI-0.35}{e_{AI}-0.35} - \frac{GI-e_{GI}}{0-e_{GI}} \\ \frac{AI-0.35}{e_{AI}-1.0} - \frac{GI-e_{GI}}{0-e_{GI}} \end{cases} \tag{6}$$

$f(\mathrm{AI}, \mathrm{GI}, e_{AI}, e_{GI})$ consists of two different threshold lines, including Threshold line 1 and 2 that show a negative relationship between aridity and optimal grazing pressure (Supplementary Fig. 8a and b). The Akaike Information Criterion (AIC) was used to determine the equation that best fitted our data[59]. Detection of the final e_{AI} and e_{GI} was conducted to determine the corresponding (e_{AI}, e_{GI}), whereby the loglikelihood value of the best threshold model was largest among all (e_{AI}, e_{GI}) pairs. Finally, violin diagrams were generated to show the differences in the predicted value at each side of every threshold line (detailed in Equation (6)).

Distribution of all variables was determined using the gmdistribution.fit function in MATLAB (The MathWorks Inc., Natick, Massachusetts, USA). Log transformation of the variables was used to reduce the conditional variance across the aridity or grazing gradient. When a variable follows a bimodal distribution, threshold regressions cannot identify breaks in continuous trends, as linear regressions depend on changes of the mean. In this case, the analysis needs to focus on the central tendency of the variable, rather than on the mean. Consequently, we used quantile regressions instead of regular linear regressions for identifying abrupt changes and thresholds along the aridity or grazing gradients evaluated. Quantile regression can down weight outliers, and correct the maximum likelihood estimation of linear models that rely on ordinary least squares of the residuals[37]. This methodological approach is highly suitable for identifying thresholds in response variables[37], and has already been used in ecological studies for doing so[11,39].

To further test whether the identified thresholds significantly affected the slope and/or intercept of the fitted regressions, we bootstrapped linear regressions at both sides of each threshold for each variable following the method reported by Berdugo, et al. [11]. Subsequently, we extracted the slope and the predicted value of the variable evaluated before and after the threshold and compared them using a Mann-Whitney U test.

Mapping 'safe operating space' for grazing under current and climate change conditions

The 'safe operating space' for grazing was determined as the maximum allowable grazing pressure that prevented key structural and functional ecosystem attributes to cross thresholds under a given aridity level. It was determined by the negative relationship between aridity and optimal grazing pressure that includes two scenarios based on data distribution: a) the shaded area below the threshold line (Threshold line 1) is regarded as the 'safe operating space', in which for a particular aridity level there is a maximum allowable grazing pressure (Supplementary Fig. 8a); and b) the shaded area above the threshold line (Threshold line 2) is regarded as the ‘unsafe operating space’, and the maximum allowable grazing pressure for a particular aridity is determined by 500 (the upper limit of the data)-current grazing level (Supplementary Fig. 8b). To estimate the ‘safe operating space’, we combined Threshold line 1 and Threshold line 2 (Supplementary Fig. 8 and Extended Data Table 1). The result showed that the ‘safe operating space’ determined by Threshold line 1 was within and smaller than that determined by Threshold 2 (Extended Data Table 1). Consequently, after combining the two, it was found that Threshold line 1 was better to capture the ‘safe operating space’ for grazing. In Threshold line 1, the ecosystem variables (i.e., plant cover) showed a decreased trend with increasing aridity, and a negative relationship was observed between aridity and optimal grazing pressure. We compared the current grazing level with the maximum allowable grazing pressure as obtained by the equation of Threshold line 1, and calculated the difference and its spatial pattern (Fig. 3 and Extended Data Fig. 3). Positive or negative values showed that the maximum allowable grazing pressure was higher or lower than the current grazing pressure, respectively. We also identified the areas that were not suitable for grazing (i.e., where the aridity was beyond the range of Threshold line 1 equation). Specially, for areas with aridity ranging from A0 (determined by the one-dimensional threshold model without the effect of grazing) to 1.0 (Supplementary Fig. 8) where there is grazing pressure in the current situation, grazing is not recommended so as to prevent key ecosystem attributes from crossing the thresholds. Under future climate conditions, we firstly determined the maximum allowable grazing pressure based on the equation of Threshold line 1 and future aridity data through simulations using the Fifth Coupled Model Intercomparison Project (CMIP5) representative concentration pathways (RCPs) RCP8.5 and RCP4.5[9]. The projected maximum allowable grazing pressure was then compared with the current grazing level to identify the areas where current grazing pressure should be reduced or increased with future climate change. By doing this, we identified areas where grazing is not recommended, areas where grazing pressure should be reduced, and areas where stocking rates could be increased. All maps were visualized in ArcGIS 10.7. (ESRI, USA).

Data Availability

The datasets analyzed in this study are publicly available, with data sources for each indicator described in the Data collection subsection of Methods in the manuscript and summarized in Supplementary Table 1. The data that support the findings of this study are available from figshare https://doi.org/10.6084/m9.figshare.22678999.

Code Availability

All data processing and analysis were conducted in ArcGIS (version 10.7), Microsoft Excel (version 2022), Origin (version 2022b), chngpt and gam packages in R (version 4.1.2), and MATLAB (version 2020a). The code used in this study is available from figshare https://doi.org/10.6084/m9.figshare.22678999.

Acknowledgements

This research is jointly funded by the National Natural Science Foundation of China Project (grant 41991235), China's Second Scientific Research Project on the Qinghai-Tibet Plateau (grant 2019QZKK0405), and the Fundamental Research Funds for the Central Universities. FTM is supported by Generalitat Valenciana (CIDEGENT/2018/041), the Spanish Ministry of Science and Innovation (EUR2022-134048) and by the contract between ETH Zurich and University of Alicante "Mapping terrestrial ecosystem structure at the global scale". ERC was supported by the Ramon y Cajal fellowship (RYC2020-030762-I) and by the CRUST R-Forze (PID2021-127631NA-I00) project founded by FEDER/Ministerio de Ciencia e Inovacion-Agencia Estatal de Investigación. Many thanks to Alistair William Robin Seddon at University of Bergen (Norway) for sharing the global Vegetation Sensitivity Index dataset.

Author Contributions Statement

C.L., B.F., S.W., F.T.M. and L.S. conceived and designed the study. C.L. carried out the calculations, drafted the figures and wrote the first draft of the manuscript. W.Z., Z.R., M.H., and Y.Z. undertook data analysis and figure reproduction. B.F., S.W., L.S., E.R.C., B.W. and F.T.M. reviewed and edited the manuscript before submission. All authors made substantial contributions to the discussion of content.

Competing Interests Statement

The authors declare no competing interests.

Figure Legends

Fig. 1. Nonlinear responses of multiple ecosystem variables to the joint effects of aridity and grazing pressure. Examples of two-dimensional thresholds observed for Vegetation cover (a), Plant species richness (b), Soil carbon content (c), Soil nitrogen content (d), NDVI (e), Carbon sequestration (f), Biocrust cover (g), Inter-annual variation of precipitation (h), and Root-shoot ratio (i). Brown and blue planes represent segmented regressions and fitted planes at both sides of each threshold line (red line).

Fig. 2. Combined effects of aridity and grazing on ecosystem structure and functioning across China's drylands. a-b: the threshold lines showing the negative relationship between aridity and optimal grazing pressure. Green and red lines showed the synergistic and contrasting effect of aridity and grazing pressure on thresholds, respectively. Blue lines are those for the Threshold line 1 and 2 which reflects the total average. The linear relationship between aridity (*Ar*) and maximum allowable grazing pressure (*Gr*) for both Threshold line 1 and 2 and their sub-types are given in the Extended Data Table 1, which was determined by the thresholds of aridity and grazing pressure and their relationship for each variable as shown in Supplementary Table 6. c: The synergistic effect of aridity and grazing reduced vegetation cover, plant species richness, soil carbon and nitrogen content, and increased the root-shoot ratio. Under this condition increases in grazing pressure located aridity thresholds at lower aridity values. Low to moderate grazing moderates the effects of aridity in reducing carbon sequestration and above-ground carbon density, making aridity thresholds occur at higher aridity values. For ecosystem variables such as biocrust cover and inter-annual precipitation variability, grazing had no effect on the aridity thresholds observed, suggesting no interaction between aridity and grazing.

Fig. 3. Future changes and climate change vulnerability in China's drylands. a: Predicted areas with the difference between maximum allowable grazing pressure and current grazing pressure in China's drylands. The blue shading with positive values and brown shading with negative values denotes where the maximum allowable grazing pressure is higher and lower than the current grazing level, respectively. The red lines denote the baseline drylands in 1950–2000 that are not suitable for grazing and thus where grazing is not recommended (i.e., their maximum allowable grazing pressure is equal to zero and the current grazing pressure leads to ecosystem thresholds to be crossed). The grey shading denotes drylands where the land covers are croplands, wetlands, or urban areas. The unshaded areas are not drylands today and therefore are outside of the range. b: Temporal

variation in the mean maximum allowable grazing pressure in China's drylands. The thin solid lines and shading are mean values and the 95% confidence intervals of 20 CMIP5 climate models, respectively. Bold solid lines show the grazing pressure trends by twenty-year running means. The horizontal solid line shows the current mean grazing pressure in China's drylands. c-d: Predicted areas with the difference between maximum allowable grazing pressure and current grazing pressure by the CMIP5 scenarios (c) RCP4.5 (i.e., assuming saturated increase in CO_2 emissions) and (d) RCP8.5 (i.e., assuming sustained increase in CO_2 emissions) by 2100 in China's drylands. The base map was obtained from the Global Aridity Index database[42] and China Data Lab[60].

References

1 Prăvălie, R. Drylands extent and environmental issues. A global approach. *Earth-Science Reviews* **161**, 259-278 (2016).

2 Reynolds, J. F. *et al.* Global desertification: building a science for dryland development. *Science* **316**, 847-851 (2007).

3 Stringer, L. C. *et al.* Climate change impacts on water security in global drylands. *One Earth* **4**, 851-864 (2021).

4 Ahlström, A. *et al.* The dominant role of semi-arid ecosystems in the trend and variability of the land CO2 sink. *Science* **348**, 895-899 (2015).

5 Poulter, B. *et al.* Contribution of semi-arid ecosystems to interannual variability of the global carbon cycle. *Nature* **509**, 600-603 (2014).

6 Maestre, F. T. *et al.* Biogeography of global drylands. *New Phytologist* **231**, 540-558 (2021).

7 D'Odorico, P., Bhattachan, A., Davis, K. F., Ravi, S. & Runyan, C. W. Global desertification: drivers and feedbacks. *Advances in Water Resources* **51**, 326-344 (2013).

8 Huang, J., Yu, H., Dai, A., Wei, Y. & Kang, L. Drylands face potential threat under 2 C global warming target. *Nature Climate Change* **7**, 417-422 (2017).

9 Huang, J., Yu, H., Guan, X., Wang, G. & Guo, R. Accelerated dryland expansion under climate change. *Nature Climate Change* **6**, 166 (2016).

10 Seddon, A. W., Macias-Fauria, M., Long, P. R., Benz, D. & Willis, K. J. Sensitivity of global terrestrial ecosystems to climate variability. *Nature* **531**, 229-232 (2016).

11 Berdugo, M. *et al.* Global ecosystem thresholds driven by aridity. *Science* **367**, 787-790 (2020).

12 Maestre, F. T. *et al.* Structure and functioning of dryland ecosystems in a changing world. *Annual Review of Ecology,*

Evolution, Systematics 47, 215-237 (2016).

13 Berdugo, M., Kéfi, S., Soliveres, S. & Maestre, F. T. Plant spatial patterns identify alternative ecosystem multifunctionality states in global drylands. *Nature Ecology & Evolution* 1, 0003 (2017).

14 Wang, C. *et al.* Aridity threshold in controlling ecosystem nitrogen cycling in arid and semi-arid grasslands. *Nature Communications* 5, 4799 (2014).

15 Delgado-Baquerizo, M. *et al.* Decoupling of soil nutrient cycles as a function of aridity in global drylands. *Nature* 502, 672-676 (2013).

16 Scheffer, M., Carpenter, S., Foley, J. A., Folke, C. & Walker, B. Catastrophic shifts in ecosystems. *Nature* 413, 591-596 (2001).

17 Scheffer, M. & Carpenter, S. R. Catastrophic regime shifts in ecosystems: linking theory to observation. *Trends in Ecology & Evolution* 18, 648-656 (2003).

18 Rockström, J. *et al.* A safe operating space for humanity. *Nature* 461, 472-475 (2009).

19 Scheffer, M. *et al.* Early-warning signals for critical transitions. *Nature* 461, 53-59 (2009).

20 Gaitán, J. J. *et al.* Aridity and overgrazing have convergent effects on ecosystem structure and functioning in Patagonian rangelands. *Land Degradation & Development* 29, 210-218 (2018).

21 Lohmann, D., Tietjen, B., Blaum, N., Joubert, D. F. & Jeltsch, F. Shifting thresholds and changing degradation patterns: climate change effects on the simulated long‐term response of a semi‐arid savanna to grazing. *Journal of Applied Ecology* 49, 814-823 (2012).

22 Ruppert, J. C. *et al.* Quantifying drylands' drought resistance and recovery: the importance of drought intensity, dominant life history and grazing regime. *Global Change Biology* 21, 1258-1270 (2015).

23 Dudney, J. & Suding, K. N. The elusive search for tipping points. *Nature Ecology & Evolution*, 1-2 (2020).

24 Maestre, F. T. *et al.* Grazing and ecosystem service delivery in global drylands. *Science* 378, 915-920 (2022).

25 Vandandorj, S., Eldridge, D. J., Travers, S. K. & Delgado‐Baquerizo, M. Contrasting effects of aridity and grazing intensity on multiple ecosystem functions and services in Australian woodlands. *Land Degradation & Development* 28, 2098-2108 (2017).

26 Li, C. *et al.* Drivers and impacts of changes in China's drylands.

Nature Reviews Earth & Environment **2**, 858-873, doi:10.1038/s43017-021-00226-z (2021).

27 Mirzabaev, A. *et al.* Cross-Chapter Paper 3: Deserts, Semi-Arid Areas and Desertification. (Cambridge University Press, In Press., 2022).

28 Shukla, P. R. *et al.* Climate Change and Land: an IPCC special report on climate change, desertification, land degradation, sustainable land management, food security, and greenhouse gas fluxes in terrestrial ecosystems. (2019).

29 Prăvălie, R., Bandoc, G., Patriche, C. & Sternberg, T. Recent changes in global drylands: Evidences from two major aridity databases. *Catena* **178**, 209-231 (2019).

30 Herrero‐Jáuregui, C. & Oesterheld, M. Effects of grazing intensity on plant richness and diversity: A meta‐analysis. *Oikos* **127**, 757-766 (2018).

31 Milchunas, D. G. & Lauenroth, W. K. Quantitative effects of grazing on vegetation and soils over a global range of environments: Ecological Archives M063-001. *Ecological monographs* **63**, 327-366 (1993).

32 Milchunas, D. G., Sala, O. E. & Lauenroth, W. K. A generalized model of the effects of grazing by large herbivores on grassland community structure. *The American Naturalist* **132**, 87-106 (1988).

33 Oñatibia, G. R., Amengual, G., Boyero, L. & Aguiar, M. R. Aridity exacerbates grazing‐induced rangeland degradation: A population approach for dominant grasses. *Journal of Applied Ecology* **57**, 1999-2009 (2020).

34 Oñatibia, G. R., Boyero, L. & Aguiar, M. R. Regional productivity mediates the effects of grazing disturbance on plant cover and patch‐size distribution in arid and semi‐arid communities. *Oikos* **127**, 1205-1215 (2018).

35 Asner, G. P., Elmore, A. J., Olander, L. P., Martin, R. E. & Harris, A. T. J. A. R. E. R. Grazing systems, ecosystem responses, and global change. **29**, 261-299 (2004).

36 Zhang, R., Wang, J. & Niu, S. Toward a sustainable grazing management based on biodiversity and ecosystem multifunctionality in drylands. *Current Opinion in Environmental Sustainability* **48**, 36-43 (2021).

37 Cade, B. S. & Noon, B. R. A gentle introduction to quantile regression for ecologists. *Frontiers in Ecology and the Environment* **1**, 412-420 (2003).

38 Tomal, J. H. & Ciborowski, J. J. Ecological models for estimating breakpoints and prediction intervals. *Ecology & Evolution* **10**,

13500-13517 (2020).

39 Hirota, M., Holmgren, M., Van Nes, E. H. & Scheffer, M. Global resilience of tropical forest and savanna to critical transitions. *Science* **334**, 232-235 (2011).

40 Zhang, J. *et al.* Water availability creates global thresholds in multidimensional soil biodiversity and functions. *Nature Ecology & Evolution*, 1-10 (2023).

41 Wu, B. *et al.* Essential dryland ecosystem variables. *Current Opinion in Environmental Sustainability* **48**, 68-76 (2020).

42 Trabucco, A. & Zomer, R. J. (ed CGIAR Consortium for Spatial Information (CGIAR-CSI)) (Published online, available from: https://figshare.com/articles/dataset/Global_Aridity_Index_and_Potential_Evapotranspiration_ET0_Climate_Database_v2/7504448/3, 2018).

43 Liu, J. *et al.* Validation of Moderate Resolution Imaging Spectroradiometer (MODIS) albedo retrieval algorithm: Dependence of albedo on solar zenith angle. *Journal of Geophysical Research: Atmospheres* **114** (2009).

44 Abatzoglou, J. T., Dobrowski, S. Z., Parks, S. A. & Hegewisch, K. C. TerraClimate, a high-resolution global dataset of monthly climate and climatic water balance from 1958–2015. *Scientific Data* **5**, 1-12 (2018).

45 Batjes, N. H. Harmonized soil property values for broad-scale modelling (WISE30sec) with estimates of global soil carbon stocks. *Geoderma* **269**, 61-68 (2016).

46 Tucker, C. J. & Sellers, P. Satellite remote sensing of primary production. *International Journal of Remote Sensing* **7**, 1395-1416 (1986).

47 Justice, C. *et al.* An overview of MODIS Land data processing and product status. *Remote Sensing of Environment* **83**, 3-15 (2002).

48 Rodriguez-Caballero, E. *et al.* Dryland photoautotrophic soil surface communities endangered by global change. *Nature Geoscience* **11**, 185-189 (2018).

49 Ellis, E. C., Antill, E. C. & Kreft, H. All is not loss: plant biodiversity in the Anthropocene. *PloS one* **7**, p.e30535 (2012).

50 Burrell, A. L., Evans, J. P. & Liu, Y. Detecting dryland degradation using time series segmentation and residual trend analysis (TSS-RESTREND). *Remote Sensing of Environment* **197**, 43-57 (2017).

51 Abel, C. *et al.* The human–environment nexus and vegetation–rainfall sensitivity in tropical drylands. *Nature Sustainability*, 1-8 (2020).

52 Xu, J., Chen, J., Liu, Y. & Fan, F. Identification of the

geographical factors influencing the relationships between ecosystem services in the Belt and Road region from 2010 to 2030. *Journal of Cleaner Production* **275**, 124153 (2020).
53 FAO. Gridded livestock of the world 2007. 131 (Rome, 2007).
54 Robinson, T. P. *et al.* Mapping the global distribution of livestock. *PloS one* **9**, e96084 (2014).
55 Naidoo, R. *et al.* Global mapping of ecosystem services and conservation priorities. *Proceedings of the National Academy of Sciences* **105**, 9495-9500 (2008).
56 Ma, H. *et al.* The global distribution and environmental drivers of aboveground versus belowground plant biomass. *Nature Ecology & Evolution* **5**, 1110-1122 (2021).
57 Fong, Y. Tutorial for the R package chngpt. (2018).
58 Muggeo, V. M. Segmented: an R package to fit regression models with broken-line relationships. *R news* **8**, 20-25 (2008).
59 Hastie, T. J. in *Statistical models in S* 249-307 (Routledge, 2017).
60 Digital Map Database of, C. (Harvard Dataverse, 2020).

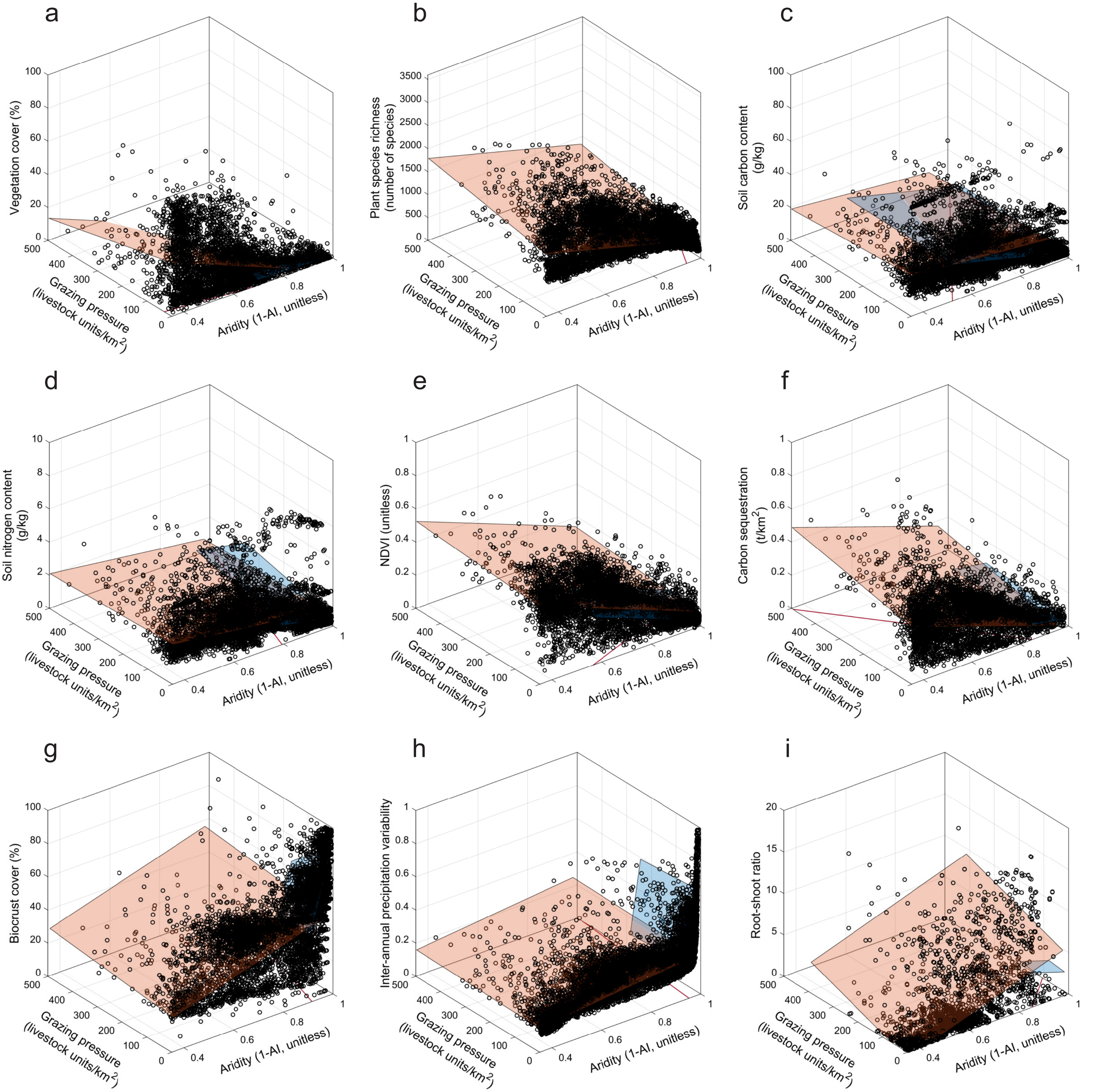

a
Vegetation cover (%)
Grazing pressure (livestock units/km^2)
Aridity (1-AI, unitless)
b
Plant species richness (number of species)
Grazing pressure (livestock units/km^2)
Aridity (1-AI, unitless)
c
Soil carbon content (g/kg)
Grazing pressure (livestock units/km^2)
Aridity (1-AI, unitless)
d
Soil nitrogen content (g/kg)
Grazing pressure (livestock units/km^2)
Aridity (1-AI, unitless)
e
NDVI (unitless)
Grazing pressure (livestock units/km^2)
Aridity (1-AI, unitless)
f
Carbon sequestration (t/km^2)
Grazing pressure (livestock units/km^2)
Aridity (1-AI, unitless)
g
Biocrust cover (%)
Grazing pressure (livestock units/km^2)
Aridity (1-AI, unitless)
h
Inter-annual precipitation variability
Grazing pressure (livestock units/km^2)
Aridity (1-AI, unitless)
i
Root-shoot ratio
Grazing pressure (livestock units/km^2)
Aridity (1-AI, unitless)

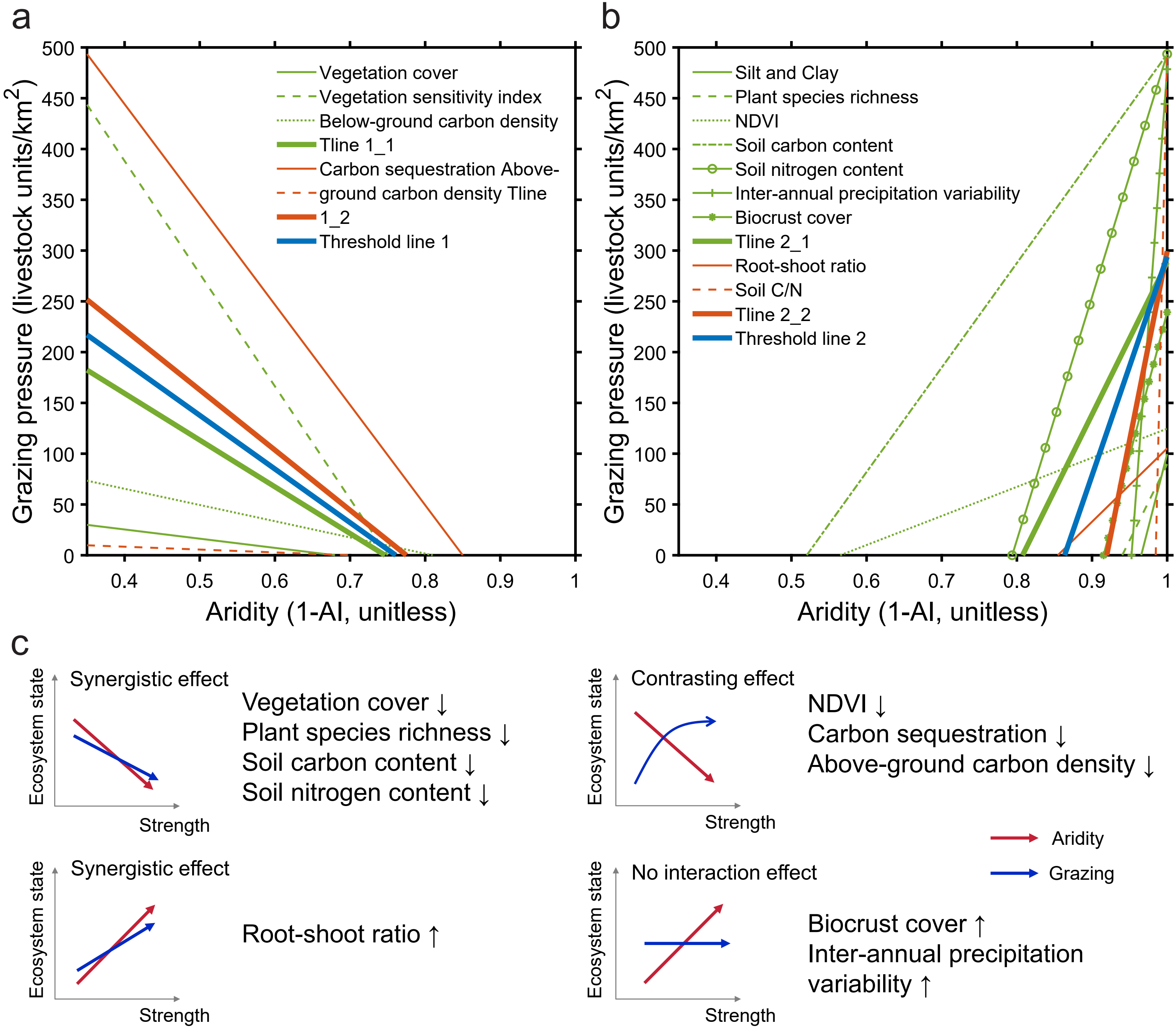
a
Grazing pressure (livestock units/km^2)
500
450
400
350
300
250
200
150
100
50
0
0.4
0.5
0.6
0.7
0.8
0.9
1
Aridity (1-AI, unitless)
Vegetation cover
Vegetation sensitivity index
Below-ground carbon density
Tline 1_1
Carbon sequestration Above-
ground carbon density Tline
1_2
Threshold line 1
b
Silt and Clay
Plant species richness
NDVI
Soil carbon content
Soil nitrogen content
Inter-annual precipitation variability
Biocrust cover
Tline 2_1
Root-shoot ratio
Soil C/N
Tline 2_2
Threshold line 2
c
Synergistic effect
Ecosystem state
Strength
Vegetation cover ↓
Plant species richness ↓
Soil carbon content ↓
Soil nitrogen content ↓
Contrasting effect
NDVI ↓
Carbon sequestration ↓
Above-ground carbon density ↓
Aridity
Grazing
Synergistic effect
Root-shoot ratio ↑
No interaction effect
Biocrust cover ↑
Inter-annual precipitation
variability ↑

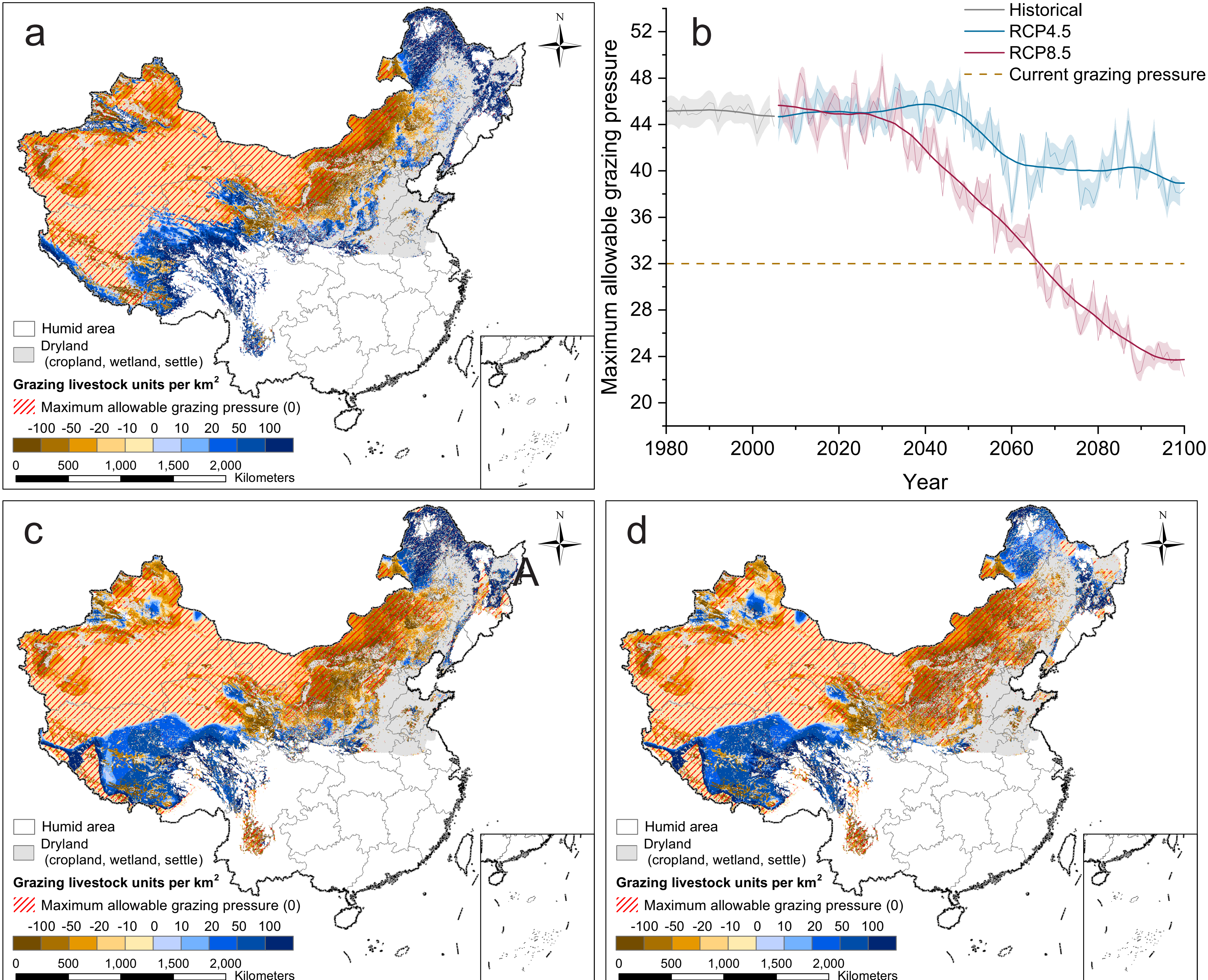
a
N
Humid area
Dryland
(cropland, wetland, settle)
Grazing livestock units per km^2
Maximum allowable grazing pressure (0)
-100 -50 -20 -10 0 10 20 50 100
0 500 1,000 1,500 2,000
Kilometers
b
Historical
RCP4.5
RCP8.5
Current grazing pressure
Maximum allowable grazing pressure
52
48
44
40
36
32
28
24
20
1980 2000 2020 2040 2060 2080 2100
Year
c
N
A
Humid area
Dryland
(cropland, wetland, settle)
Grazing livestock units per km^2
Maximum allowable grazing pressure (0)
-100 -50 -20 -10 0 10 20 50 100
0 500 1,000 1,500 2,000
Kilometers
d
N
Humid area
Dryland
(cropland, wetland, settle)
Grazing livestock units per km^2
Maximum allowable grazing pressure (0)
-100 -50 -20 -10 0 10 20 50 100
0 500 1,000 1,500 2,000
Kilometers

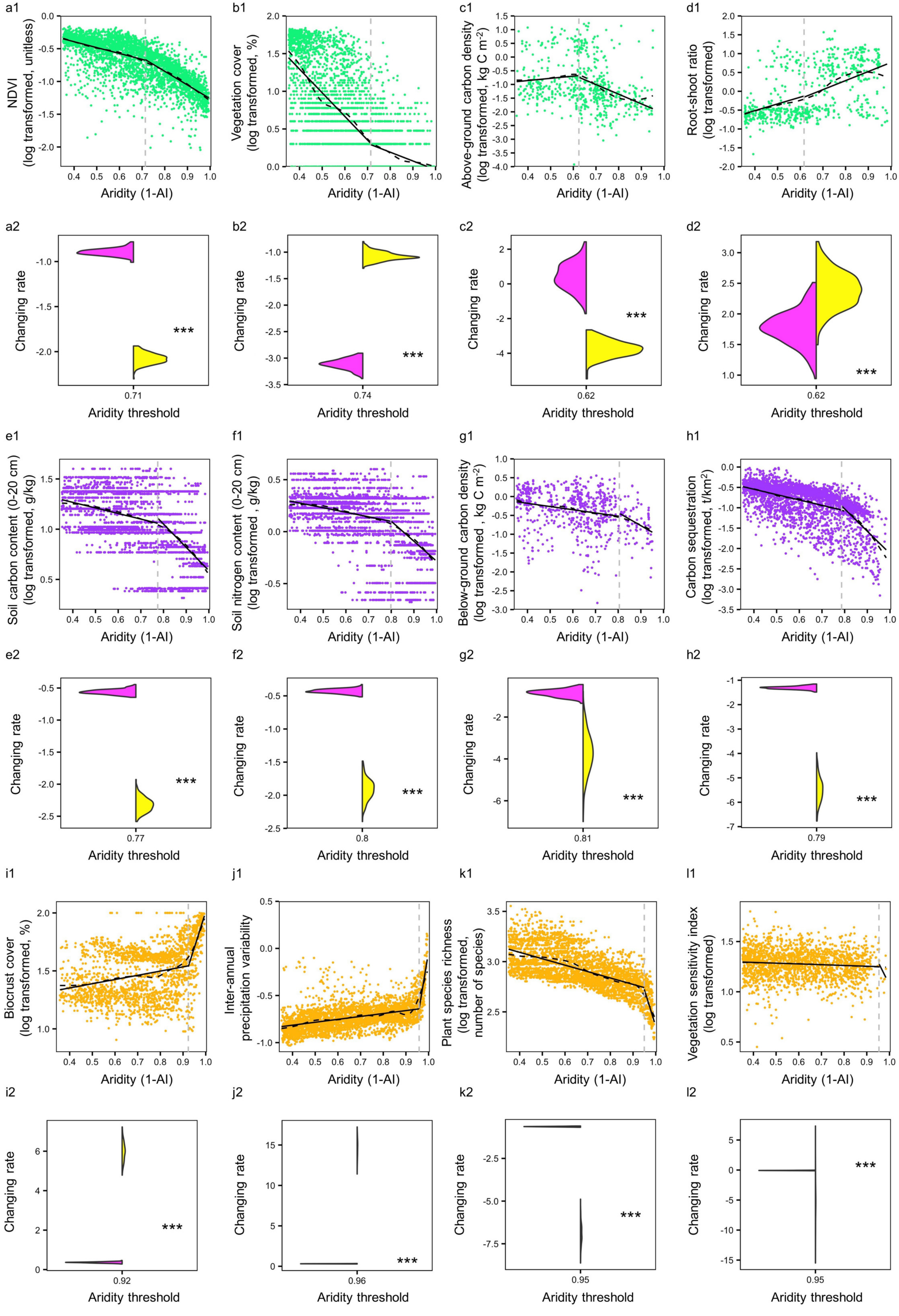
a1
NDVI (log transformed, unitless)
Aridity (1-AI)
b1
Vegetation cover (log transformed, %)
Aridity (1-AI)
c1
Above-ground carbon density (log transformed, kg C m-2)
Aridity (1-AI)
d1
Root-shoot ratio (log transformed)
Aridity (1-AI)
a2
Changing rate
***
0.71
Aridity threshold
b2
Changing rate
***
0.74
Aridity threshold
c2
Changing rate
***
0.62
Aridity threshold
d2
Changing rate
***
0.62
Aridity threshold
e1
Soil carbon content (0-20 cm) (log transformed, g/kg)
Aridity (1-AI)
f1
Soil nitrogen content (0-20 cm) (log transformed , g/kg)
Aridity (1-AI)
g1
Below-ground carbon density (log transformed , kg C m-2)
Aridity (1-AI)
h1
Carbon sequestration (log transformed, t/km2)
Aridity (1-AI)
e2
Changing rate
***
0.77
Aridity threshold
f2
Changing rate
***
0.8
Aridity threshold
g2
Changing rate
***
0.81
Aridity threshold
h2
Changing rate
***
0.79
Aridity threshold
i1
Biocrust cover (log transformed, %)
Aridity (1-AI)
j1
Inter-annual precipitation variability
Aridity (1-AI)
k1
Plant species richness (log transformed, number of species)
Aridity (1-AI)
l1
Vegetation sensitivity index (log transformed)
Aridity (1-AI)
i2
Changing rate
***
0.92
Aridity threshold
j2
Changing rate
***
0.96
Aridity threshold
k2
Changing rate
***
0.95
Aridity threshold
l2
Changing rate
***
0.95
Aridity threshold

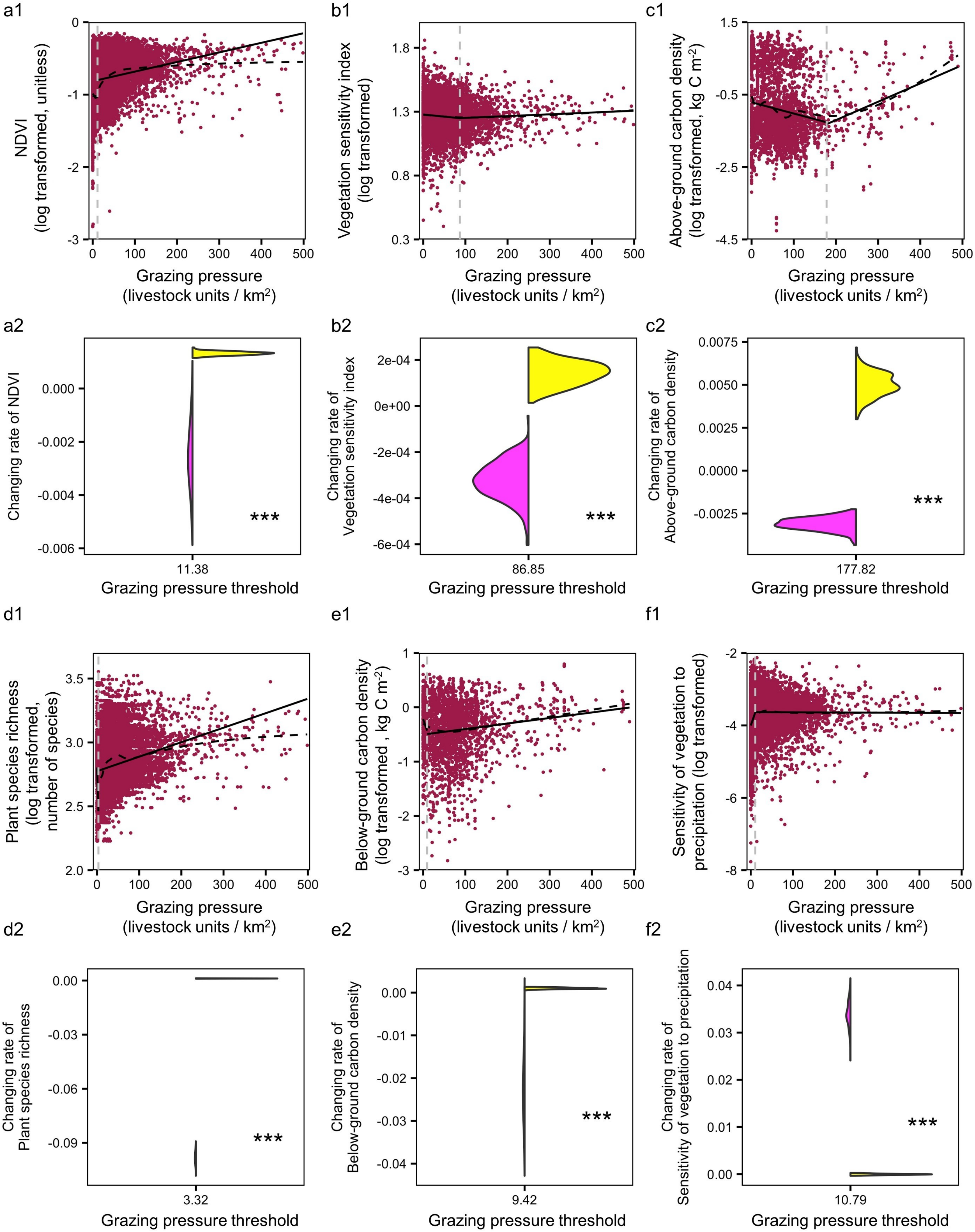

a1
NDVI (log transformed, unitless)
Grazing pressure (livestock units / km2)
b1
Vegetation sensitivity index (log transformed)
Grazing pressure (livestock units / km2)
c1
Above-ground carbon density (log transformed, kg C m-2)
Grazing pressure (livestock units / km2)
a2
Changing rate of NDVI
***
11.38
Grazing pressure threshold
b2
Changing rate of Vegetation sensitivity index
***
86.85
Grazing pressure threshold
c2
Changing rate of Above-ground carbon density
***
177.82
Grazing pressure threshold
d1
Plant species richness (log transformed, number of species)
Grazing pressure (livestock units / km2)
e1
Below-ground carbon density (log transformed , kg C m-2)
Grazing pressure (livestock units / km2)
f1
Sensitivity of vegetation to precipitation (log transformed)
Grazing pressure (livestock units / km2)
d2
Changing rate of Plant species richness
***
3.32
Grazing pressure threshold
e2
Changing rate of Below-ground carbon density
***
9.42
Grazing pressure threshold
f2
Changing rate of Sensitivity of vegetation to precipitation
***
10.79
Grazing pressure threshold

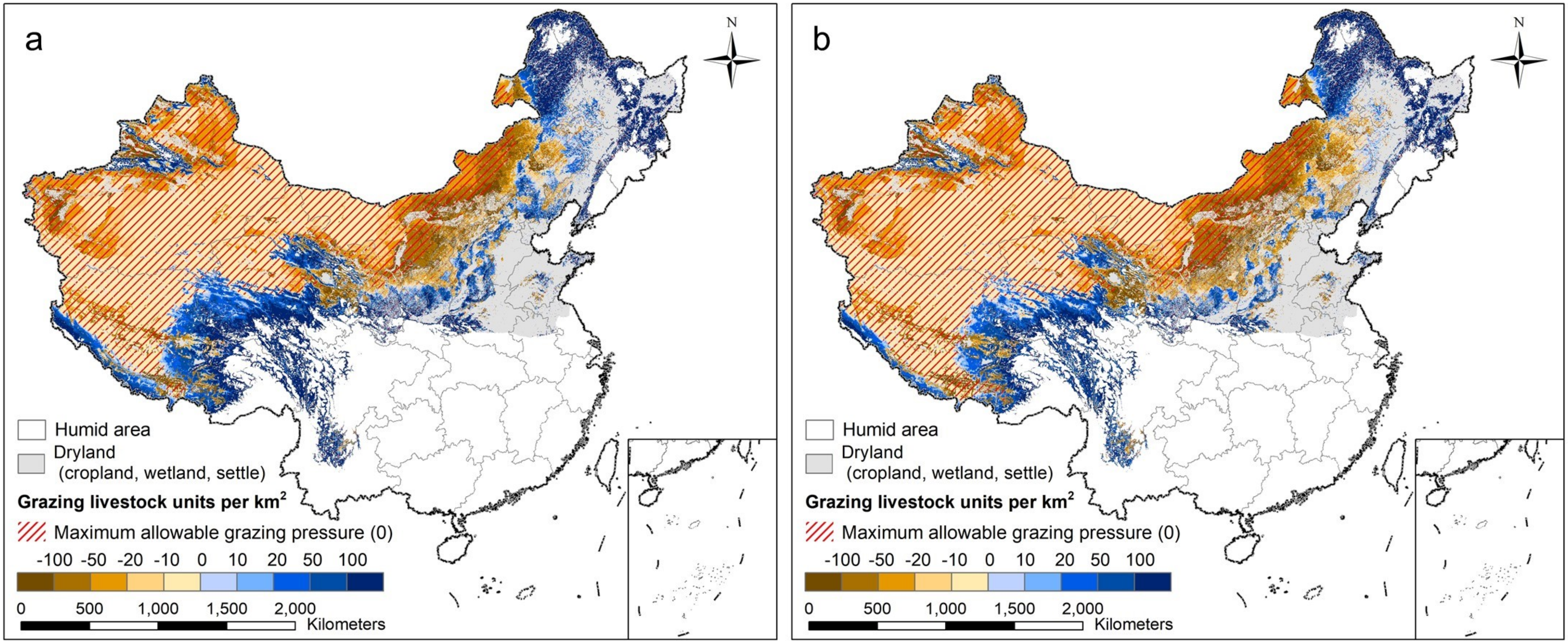
a
b
N
Humid area
Dryland
(cropland, wetland, settle)
Grazing livestock units per km²
Maximum allowable grazing pressure (0)
-100 -50 -20 -10 0 10 20 50 100
0 500 1,000 1,500 2,000
Kilometers

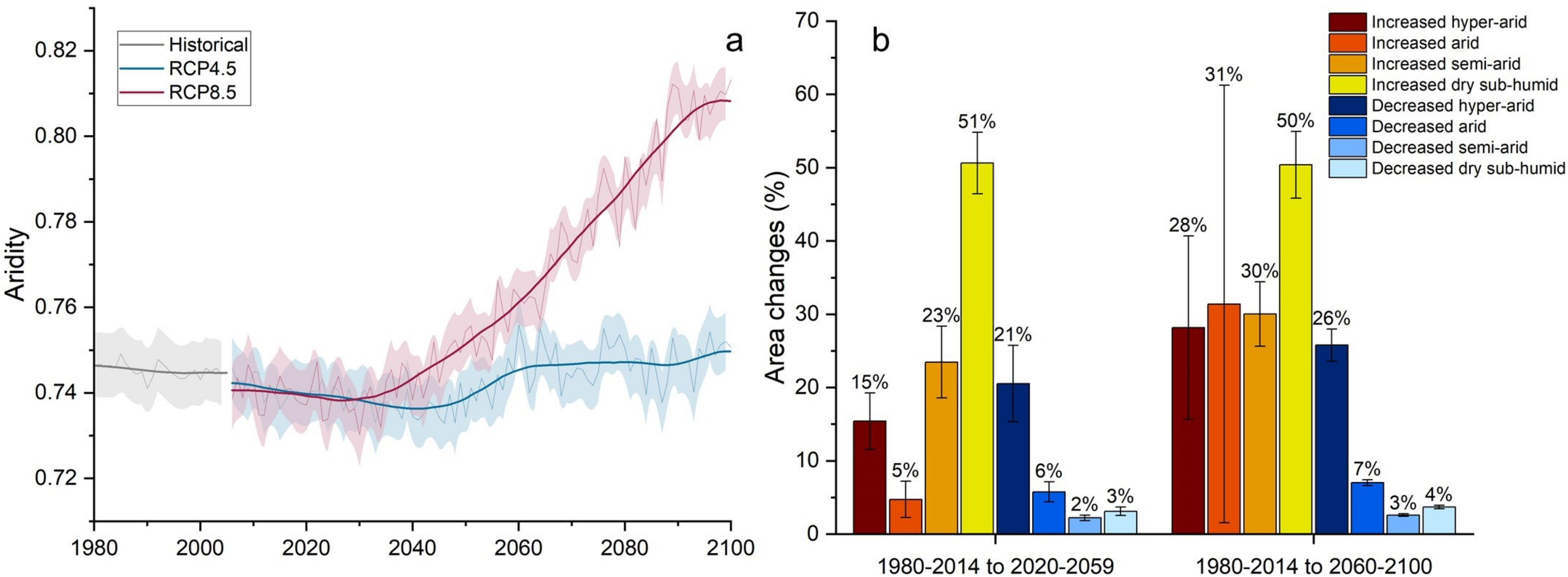

Aridity
0.82
0.80
0.78
0.76
0.74
0.72
1980
2000
2020
2040
2060
2080
2100
Historical
RCP4.5
RCP8.5
a
b
Area changes (%)
70
60
50
40
30
20
10
0
Increased hyper-arid
Increased arid
Increased semi-arid
Increased dry sub-humid
Decreased hyper-arid
Decreased arid
Decreased semi-arid
Decreased dry sub-humid
15%
5%
23%
51%
21%
6%
2%
3%
28%
31%
30%
50%
26%
7%
3%
4%
1980-2014 to 2020-2059
1980-2014 to 2060-2100

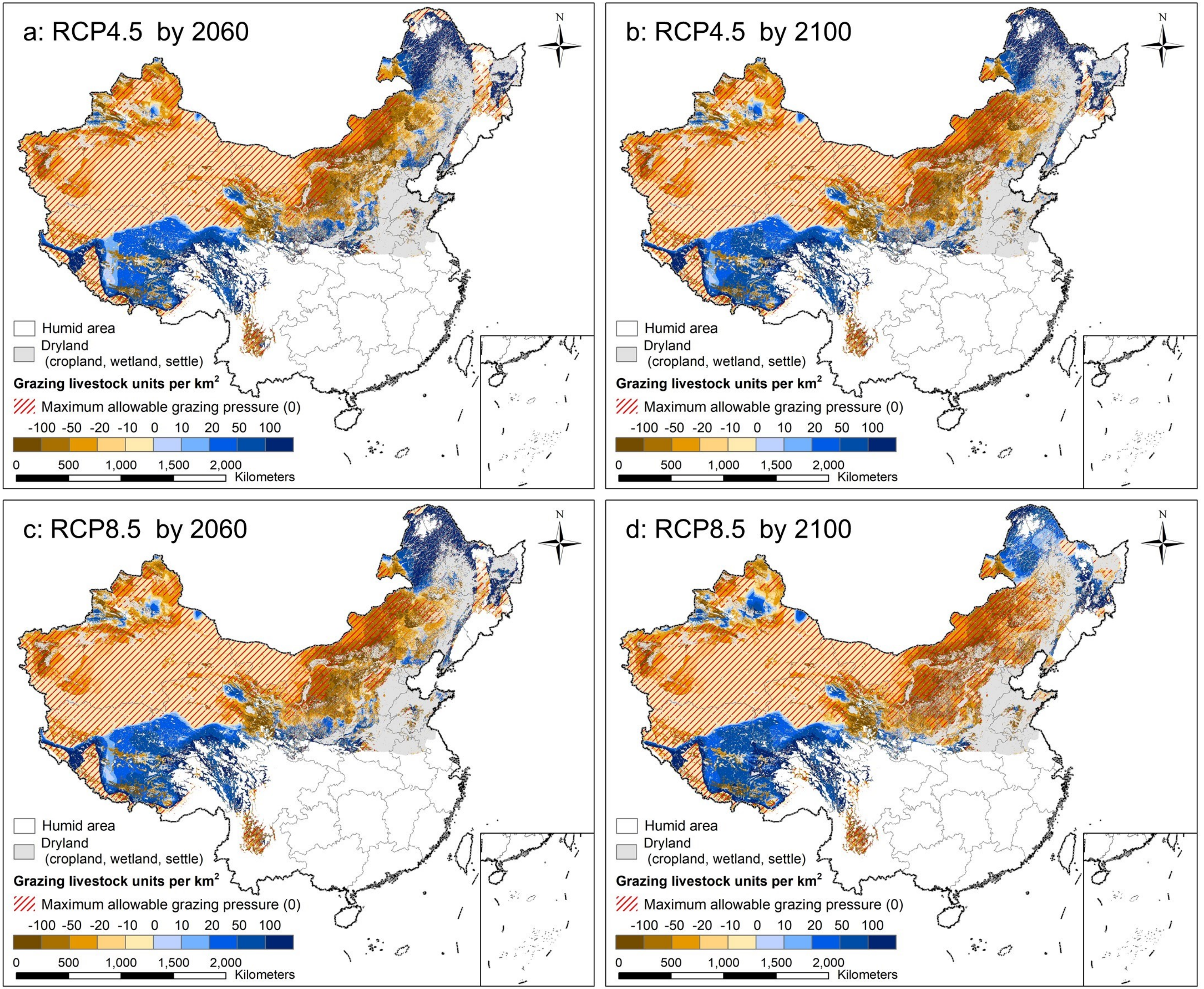
a: RCP4.5 by 2060
b: RCP4.5 by 2100
c: RCP8.5 by 2060
d: RCP8.5 by 2100
N
Humid area
Dryland
(cropland, wetland, settle)
Grazing livestock units per km2
Maximum allowable grazing pressure (0)
-100 -50 -20 -10 0 10 20 50 100
0 500 1,000 1,500 2,000
Kilometers

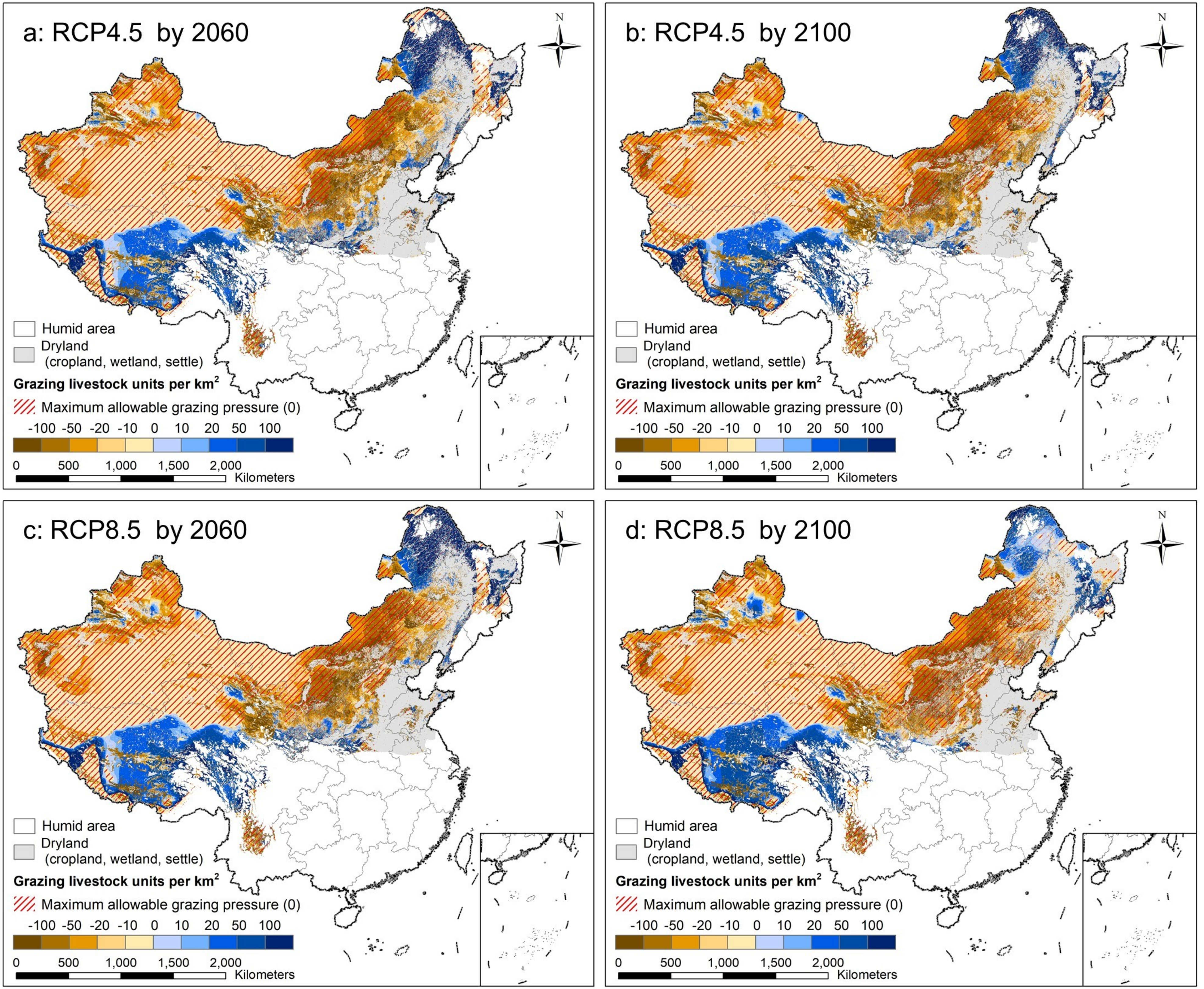
a: RCP4.5 by 2060
b: RCP4.5 by 2100
c: RCP8.5 by 2060
d: RCP8.5 by 2100
N
Humid area
Dryland
(cropland, wetland, settle)
Grazing livestock units per km²
Maximum allowable grazing pressure (0)
-100 -50 -20 -10 0 10 20 50 100
0 500 1,000 1,500 2,000
Kilometers

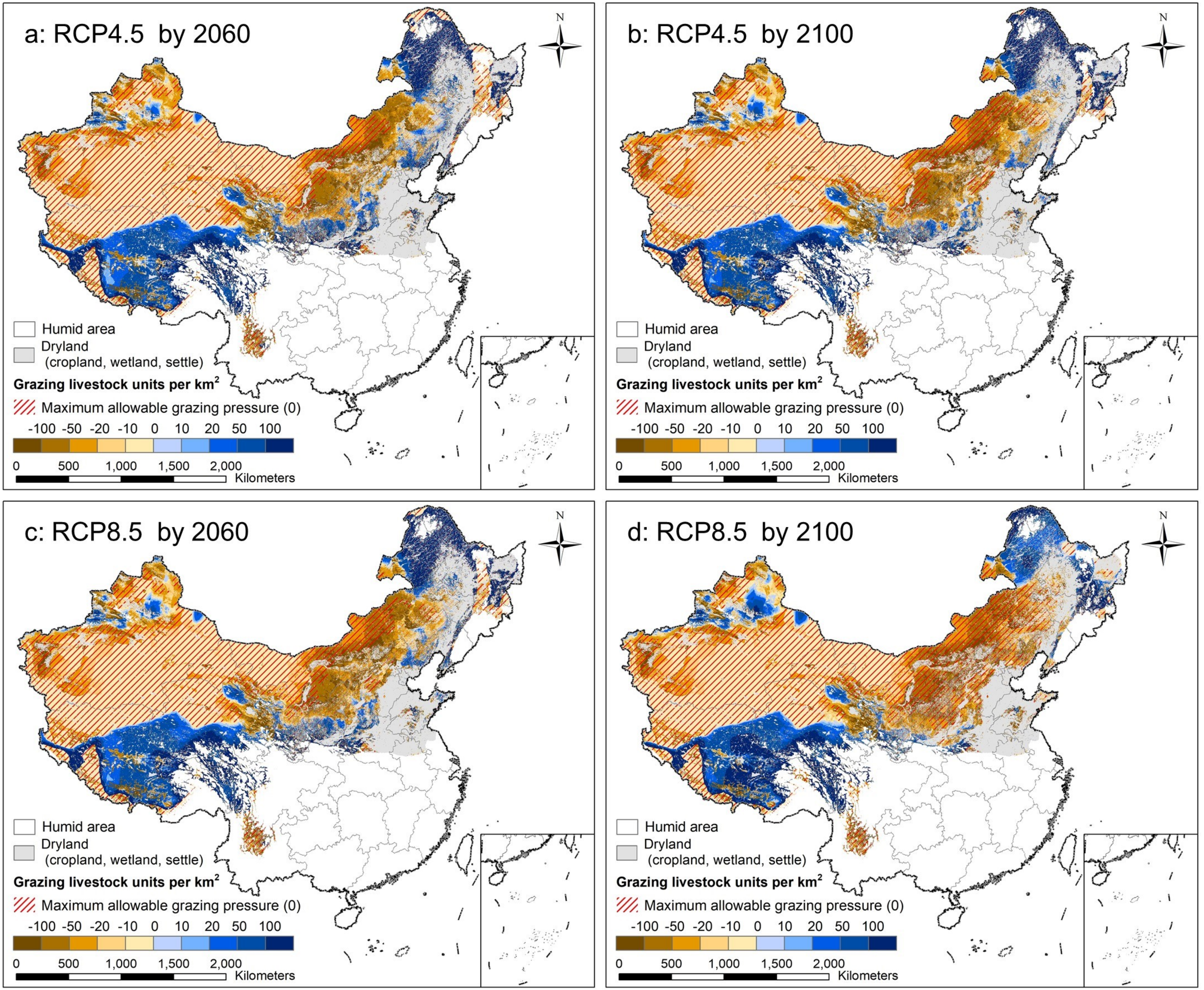
a: RCP4.5 by 2060
N
Humid area
Dryland
(cropland, wetland, settle)
Grazing livestock units per km²
Maximum allowable grazing pressure (0)
-100 -50 -20 -10 0 10 20 50 100
0 500 1,000 1,500 2,000
Kilometers
b: RCP4.5 by 2100
N
Humid area
Dryland
(cropland, wetland, settle)
Grazing livestock units per km²
Maximum allowable grazing pressure (0)
-100 -50 -20 -10 0 10 20 50 100
0 500 1,000 1,500 2,000
Kilometers
c: RCP8.5 by 2060
N
Humid area
Dryland
(cropland, wetland, settle)
Grazing livestock units per km²
Maximum allowable grazing pressure (0)
-100 -50 -20 -10 0 10 20 50 100
0 500 1,000 1,500 2,000
Kilometers
d: RCP8.5 by 2100
N
Humid area
Dryland
(cropland, wetland, settle)
Grazing livestock units per km²
Maximum allowable grazing pressure (0)
-100 -50 -20 -10 0 10 20 50 100
0 500 1,000 1,500 2,000
Kilometers

Line type	Descriptions	Linear relationship between aridity (*Ar*) and maximum allowable grazing pressure (*Gr*)
Threshold line 1	Negative relationship between aridity and optimal grazing pressure	(Ar-0.76)/(0.76-0.35)+Gr/210.06=0
Tline1_1	Synergistic effect of aridity and optimal grazing pressure	(Ar-0.74)/(0.74-0.35)+Gr/182.33=0
Tline1_2	Contrasting effect of aridity and optimal grazing pressure	(Ar-0.78)/(0.78-0.35)+Gr/251.65=0
Threshold line 2	Negative relationship between aridity and optimal grazing pressure	(Ar-0.83)/(0.83-1.00)+Gr/290.85=0
Tline2_1	Synergistic effect of aridity and optimal grazing pressure	(Ar-0.81)/(0.81-1.00)+Gr/288.41=0
Tline2_2	Contrasting effect of aridity and optimal grazing pressure	(Ar-0.92)/(0.92-1.00)+Gr/299.38=0